QUANTUM SENSING

Quantum-enhanced sensing of displacements and electric fields with two-dimensional trapped-ion crystals

Kevin A. Gilmore^{1,2}*†, Matthew Affolter¹, Robert J. Lewis-Swan^{3,4}, Diego Barberena^{5,6}, Elena Jordan¹‡, Ana Maria Rey^{5,6}*, John J. Bollinger¹*

Fully controllable ultracold atomic systems are creating opportunities for quantum sensing, yet demonstrating a quantum advantage in useful applications by harnessing entanglement remains a challenging task. Here, we realize a many-body quantum-enhanced sensor to detect displacements and electric fields using a crystal of ~150 trapped ions. The center-of-mass vibrational mode of the crystal serves as a high-Q mechanical oscillator, and the collective electronic spin serves as the measurement device. By entangling the oscillator and collective spin and controlling the coherent dynamics via a many-body echo, a displacement is mapped into a spin rotation while avoiding quantum back-action and thermal noise. We achieve a sensitivity to displacements of 8.8 ± 0.4 decibels below the standard quantum limit and a sensitivity for measuring electric fields of 240 ± 10 nanovolts per meter in 1 second. Feasible improvements should enable the use of trapped ions in searches for dark matter.

he development of protocols and quantum platforms that harness entanglement or correlations to sense or measure a physical quantity with an advantage relative to classical alternatives is of both practical and fundamental interest (1, 2). Quantum-enhanced sensors have the potential to enable the measurement of previously undetectable signals that could improve our understanding of the universe. Two prominent examples are gravitational wave detection, where nonclassical states of light are now being adopted to achieve unparalleled sensitivity (3, 4), and searches for dark matter, where a quantum advantage could enable sensing of the weak, nongravitational interaction of dark matter with normal matter (5-8).

In parallel, mechanical oscillators have become established as exquisite quantum tools to measure small displacements due to weak forces and electric fields (9–17), such as those generated by axion-like dark matter and hidden photons (18). At the simplest level, a weak, resonant force interacting with the mechanical oscillator generates a small coherent displacement β [normalized to twice the size of the oscillator's zero-point motion (19)] of the oscillator amplitude over time.

¹National Institute of Standards and Technology, Boulder, CO 80305, USA. ²Department of Physics, University of Colorado, Boulder, CO 80309, USA. ³Homer L. Dodge Department of Physics and Astronomy, University of Oklahoma, Norman, OK 73019, USA. ⁴Center for Quantum Research and Technology, University of Oklahoma, Norman, OK 73019, USA. ⁵JILA, NIST, and Department of Physics, University of Colorado, Boulder, CO 80309, USA. ⁶Center for Theory of Quantum Matter, University of Colorado, Boulder, CO 80309, USA.

*Corresponding author. Email: kevin.gilmore@colorado.edu (K.A.G.); arey@jila.colorado.edu (A.M.R.); john.bollinger@nist.gov (J.J.B.)

†Present address: Honeywell Quantum Solutions, Broomfield, CO 80021, USA. ‡Present address: Physikalisch-Technische Bundesanstalt, 38116 Braunschweig, Germany. Typically, the displacement is then inferred by making a measurement on a complementary internal or coupled degree of freedom of the system.

The precision $\Delta\beta$ to which this displacement β can be determined using classical resources that use uncorrelated states, such as a vacuum or a coherent state, is fundamentally bounded by the so-called standard quantum limit (SQL) that limits the attainable sensitivity to $\Delta\beta \geq \frac{1}{2}$. However, by introducing entanglement between the oscillator and the measurement degree of freedom before the oscillator is excited, one can attain sub-SQL precision (20–23). This requires subtle control over both the oscillator and the measurement system to minimize undesirable classical noise and to evade quantum back-action (24).

We demonstrate a quantum advantage for both displacement and electric field sensing in a two-dimensional (2D) trapped-ion crystal of ~150 ions, 200 μm in diameter. The center-ofmass (COM) normal mode of the crystal realizes the mechanical oscillator, and the internal electronic spin of the ions serves as the accessible measurement probe. A spin-dependent optical dipole force (ODF) that resonantly couples the spins and the COM mode is used to generate metrologically useful entanglement, which enables precise sensing of displacements of the oscillator (21). By implementing a many-body echo protocol (23) to subsequently disentangle the spins and the oscillator, we are able to estimate the displacement-ideally free from thermal noise-through simple global measurements of the spins. With this technique, we achieve a sensitivity of 8.8 ± 0.4 dB below the SQL for displacements and 4.0 ± 0.5 dB below the SQL for electric fields. In practical terms, we demonstrate an ultimate electric field measurement sensitivity of 240 \pm 10 nV m⁻¹/ $\sqrt{\text{Hz}}$, an improvement by a factor of 300 over prior off-resonant classical protocols in trapped ions (14, 16) and by more than an order of magnitude over state-of-the-art electrometers based on Rydberg atoms (25). Relative to similar protocols previously performed using a single Rydberg atom (22) or a single trapped ion (20, 26) to encode a spin-1/2 degree of freedom, our protocol demonstrates an enhanced sensitivity resulting from quantum entanglement in a mesoscopic ion crystal, while also benefiting from the intrinsic reduction of zero-point motion in the collective mechanical oscillator as a consequence of the large ion number.

Entanglement-enhanced sensor

Our quantum sensor consists of a single-plane Coulomb crystal of $N \sim 150^{9} \mathrm{Be^{+}}$ ions confined in a Penning trap (14, 16, 27–29) (Fig. 1). The ${}^{2}S_{1/2}$ ground-state valence electron spin $|\uparrow\rangle$ ($|\downarrow\rangle$) \equiv $|m_J = +\frac{1}{2}\rangle$ ($|m_J = -\frac{1}{2}\rangle$) encodes a spin- $\frac{1}{2}$ degree of freedom in each ion, which can be coherently controlled by external microwaves resonant with the 124-GHz frequency splitting of the electronic spin states in the presence of a B = 4.5 T magnetic field. The motion of the ion crystal can be decomposed into 2N in-plane modes and N axial modes, with the latter coupled to the spin degree of freedom by a spindependent ODF produced by a pair of offresonant laser beams detuned from the nearest optical transitions by ~20 GHz. The ODF beams generate a 1D traveling-wave potential at a frequency u, which, in contrast to prior settings for sensing in our experiment (14, 16), is now chosen to be near-resonant with the COM mode at a frequency $\omega_z/(2\pi)$ = 1.59 MHz, such that the COM is the dominant motional contribution to the observed dynamics. In this limit, and assuming that the ions have an axial extent that is small relative to the wavelength of the traveling-wave optical potential, the system can be well approximated by the Hamiltonian

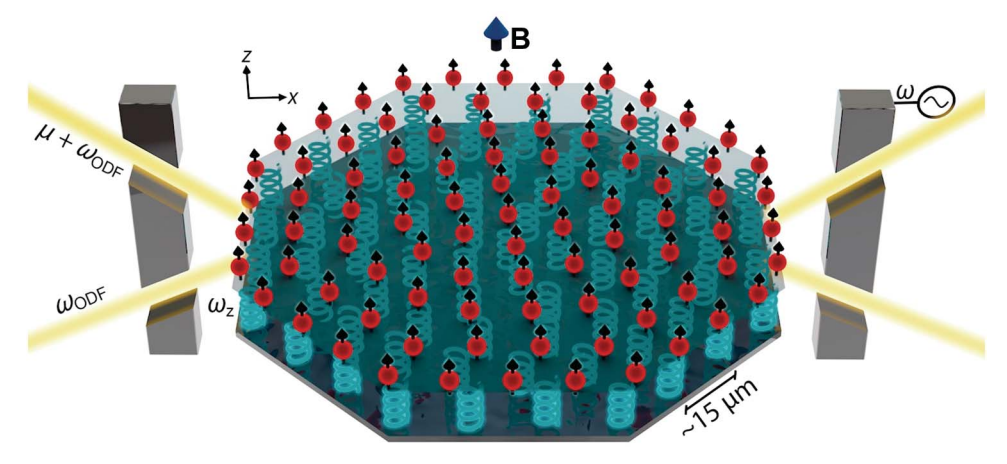
$$\hat{H}_{ ext{ODF}} = rac{\hbar g}{\sqrt{N}} \left(\hat{a} + \hat{a}^{\dagger}
ight) \hat{J}_z - \hbar \delta \hat{a}^{\dagger} \hat{a} \quad (1)$$

(19,30). Here, \hbar is the Planck constant divided by 2π ; \hat{a}^{\dagger} and \hat{a} are the COM phonon creation and annihilation operators that couple uniformly to all spins with strength g; $\delta = \mu - \omega_z$ is the detuning from the COM mode, ideally tuned to be on resonance in our protocol, $\delta = 0$; and $\hat{J}_{\alpha} = 1/2 \sum_{j=1}^{N} \hat{\sigma}_{\alpha}^{(j)}$ are the collective spin operators, where $\hat{\sigma}_{\alpha}^{(j)}$ are Pauli operators for the ith spin

In the experimental sequence to sense small displacements of the COM oscillator (Fig. 2A), the ions are prepared in the state $|\uparrow\rangle_N$ by optical pumping before a microwave $\pi/2$ pulse is applied to rotate the spins to align along the

Fig. 1. Trapped-ion crystal quantum sensor.

An ensemble of beryllium ions (red dots) confined within a Penning trap self-arrange into a 2D triangular lattice. The Penning trap is characterized by axial magnetic field B = 4.45 Tand axial trap frequency $\omega_z = 2\pi \times 1.59$ MHz. Cylindrical electrodes (cross section shown. in gray) generate a harmonic confining potential along the \hat{Z} axis, whereas radial confinement is provided by the Lorentz force from $\mathbf{E} \times \mathbf{B}$ -induced rotation in the axial magnetic field. The valence electron spin (black arrows) of the ions realizes a collective spin that serves as the measurement device. The center-of-mass (COM) motional mode of the ion crystal realizes a high-Q mechanical oscillator (blue springs) with frequency ω_z .



Crossed optical beams (yellow lines) with a beat-note frequency $\mu \approx \omega_z$ generate a spin-dependent optical-dipole force that couples the spins and the COM oscillator. An AC voltage source is applied to the trap endcap electrode to generate a coherent axial oscillation with calibrated amplitude Z_c and frequency $\omega = \omega_z$.

 \hat{x} axis of the Bloch sphere. To entangle the spins and the phonons, we apply the ODF Hamiltonian (\hat{H}_{ODF}) for time τ. Then, a calibrated AC voltage is applied to an endcap electrode for a time $t_{\text{drive}} \ll \tau$ to drive up a small coherent displacement β of the COM oscillator. Recent work (16) has established a stable relative phase between the displacement β and the ODF, which is experimentally optimized to ensure the largest signal. To optimally detect the displacement, we implement a many-body echo to undo the entangling dynamics by applying a second ODF drive with opposite sign $-\hat{H}_{ODF}$ for an identical time τ . Experimentally this is done by applying a microwave π pulse about the \hat{x} axis to map $|\uparrow\rangle \rightarrow |\downarrow\rangle$, which is equivalent to setting $g \rightarrow -g$. Finally, the displacement is estimated via a projective measurement on the spin degree of freedom. Specifically, to make an effective measurement of \hat{J}_y , we rotate the spins by a microwave $\pi/2$ pulse about the \hat{x} axis and then measure J_z using state-dependent fluorescence imaging (19).

To simplify our analysis of the experimental protocol, we assume that the ions are initialized in the motional ground state, such that the state of the spins and COM mode after the first microwave pulse is $|\psi(0)\rangle=|0\rangle_b\otimes|\langle N/2\rangle_x\rangle$. Here, we describe the spins using Dicke states $\hat{J}_\alpha|m_\alpha\rangle=m_\alpha|m_\alpha\rangle$ with $\alpha=x,y,z$ and $|0\rangle_b$ is the bosonic vacuum. The first ODF generates a spin-dependent coherent displacement of the oscillator.

$$egin{aligned} |\psi_{
m in}
angle &= \expiggl[-irac{\hbar g au}{\sqrt{N}} \Big(\hat{a}+\hat{a}^\daggeriggr)\hat{J}_z\Big] |\psi(0)
angle \ &= \sum_{m_z=-N/2}^{N/2} c_{m_z} |lpha_{m_z}
angle_b \otimes |m_z
angle \end{aligned}$$

resulting in strong spin-motion entanglement. This can be directly quantified by the purity of the reduced density matrix of the oscillator

degree of freedom after tracing over the spin [e.g., Rényi entanglement entropy S_2 (19)] during the first ODF sequence, as shown in Fig. 2B. In Eq. 2 we introduce $|\alpha_{m_z}\rangle_b$ as coherent states with complex amplitude $\alpha_{m_z}=-im_z g \tau/\sqrt{N}$, and c_{m_z} are defined as the expansion coefficients $\left|(N/2)_x\right>\equiv \sum_{m_z} c_{m_z} |m_z\rangle$.

Because $N \gg 1$ in our 2D trapped-ion crystal, we are able to formulate a particularly simple understanding of the metrological utility of the spin-boson entanglement created in the state $|\psi_{in}\rangle.$ The ODF Hamiltonian can be approximately recast as a squeezing Hamiltonian, $\hat{H}_{\text{ODF}} \equiv g(\hat{x}_+^2 - \hat{x}_-^2)/2$, where $\hat{x}_\pm = \pm (\hat{a} + \hat{a}^\dagger \pm \sqrt{4/N}\hat{J}_z)/2$ and $\hat{p}_\pm = \pm i(\hat{a}^\dagger - \hat{a}^\dagger)/2$ $\hat{a} \pm i\sqrt{4/N}\hat{J}_y)/2$. Here, \hat{x}_{\pm} and \hat{p}_{\pm} are quadrature operators of a pair of effective oscillators resulting from a hybridization of the spin and boson degrees of freedom. Note that the normalization of the spin operators in the definition of \hat{x}_{+} and \hat{p}_{+} means that the $\sim \sqrt{N}$ projection noise of the original coherent spin state contributes $\sim \mathcal{O}(1)$ noise to the hybrid quadratures, similar to the vacuum noise of the mechanical oscillator. In this language, the action of \hat{H}_{ODF} is to generate squeezing along specific quadratures in the independent (\hat{x}_+, \hat{p}_+) and (\hat{x}_-, \hat{p}_-) phase spaces (Fig. 2C). In the original basis of the spin and boson degrees of freedom, this squeezing manifests as strong correlations and entanglement between the spins and bosons.

The subsequently applied displacement of the COM oscillator, assumed to be orthogonal to the spin-dependent displacements, is described by the unitary transformation $\hat{U}_{\beta} = \exp[\beta(\hat{a} - \hat{a}^{\dagger})] = \exp(i\sqrt{2}\beta\hat{p}_b), \text{ where } \sqrt{2}i\hat{p}_b = \hat{a} - \hat{a}^{\dagger} \left(\sqrt{2}\hat{x}_b = \hat{a} + \hat{a}^{\dagger}\right) \text{ are the oscillator quadratures. This leads to the displaced state } |\psi^{\beta}_{n}\rangle = \hat{U}_{\beta}|\psi_{in}\rangle, \text{ which can be equivalently framed as a shift in the spin-boson quadrature } \hat{x}_{+} \rightarrow \hat{x}_{+} + \beta/\sqrt{2} \quad (\hat{x}_{-} \rightarrow \hat{x}_{-} - \beta/\sqrt{2}).$ The squeezing generated by the initial ODF

drive means that, in principle, a small displacement quickly leads to a state that is distinguishable from $|\psi_{\rm in}\rangle$. This displacement, parametrized by β , can be estimated with a sensitivity (see Fig. 2) limited by the quantum Cramer-Rao bound for displacements (31), $(\Delta\beta)^2=1/(4+4g^2\tau^2)$ (19). This bound can be recast in the more familiar form of the Heisenberg limit for displacements, $(\Delta\beta)^2_{\rm HL}\approx 1/n$ (21), where $n\sim g^2\tau^2$ is the occupancy of the effective oscillator before the displacement. This is to be contrasted with the SQL for displacements $(\Delta\beta)^2_{\rm SQL}=1/4$, which is the sensitivity attainable with a coherent state

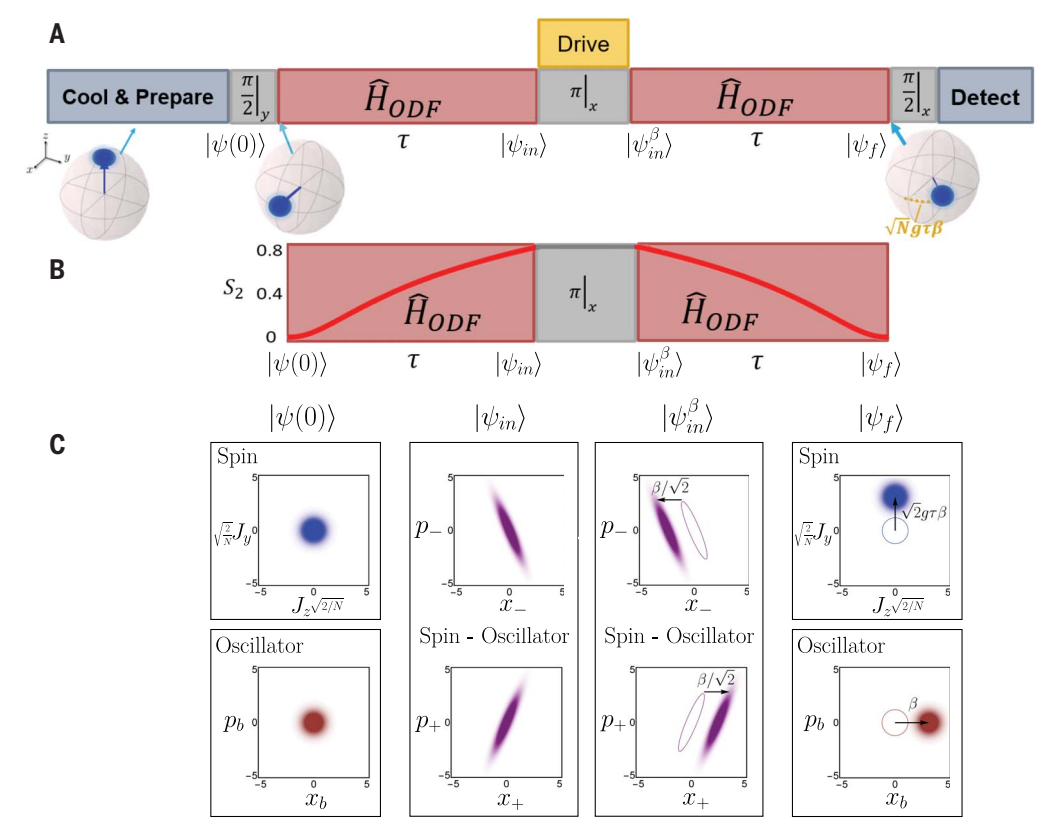
Nonetheless, fully attaining the sensitivity promised by the state $|\psi_{in}\rangle$ is not straightforward. In particular, the high degree of spin-boson entanglement in $|\psi_{in}\rangle$ means that a simple measurement of either the spins or phonons independently is insufficient to precisely infer β (19). Instead, a more sophisticated measurement that accounts for correlations between the degrees of freedom is required. We address this challenge and remove undesirable quantum back-action effects by the application of a time-reversal step that perfectly disentangles the spin and the oscillator (see Fig. 2) and maps the displacement to accessible spin observables. Specifically, the final state, obtained after applying the many-body echo to $|\psi_{in}^{\beta}\rangle$ (Eq. 2), is equivalent to

$$\begin{split} |\psi_{\rm f}\rangle &= \exp \left[i \frac{\hbar g \tau}{\sqrt{N}} \left(\hat{a} + \hat{a}^{\dagger} \right) \hat{J}_z \right] \left| \psi_{\rm in}^{\beta} \right\rangle \\ &= \exp \left(\frac{2 i g \tau \beta}{\sqrt{N}} \hat{J}_z \right) \hat{U}_{\beta} |\psi(0)\rangle \end{split} \tag{3}$$

(19). Writing the final state in the latter form demonstrates the power of the many-body

Fig. 2. Displacement-sensing protocol.

(A) The ions are Doppler-cooled and optically pumped into the state $|\uparrow\rangle$, and a microwave $\pi/2$ pulse then rotates the spin ensemble to align along the \hat{x} axis to prepare the initial state $|\psi(0)\rangle$. A resonant ODF drive, described by \hat{H}_{ODF} (Eq. 1), is then applied for a duration τ to yield the state $|\psi_{in}\rangle$ in which the spin and the COM oscillator are entangled. To generate a small spin-independent displacement B of the oscillator, we apply a weak drive to an endcap electrode resonant with the COM frequency, yielding the perturbed state $|\psi_{in}^{\beta}\rangle$. Simultaneously, a π pulse is applied to flip $|\uparrow\rangle \rightarrow |\downarrow\rangle$ and thus effectively reverse the sign of \hat{H}_{ODF} when a subsequent resonant ODF drive is applied. A final $\pi/2$ pulse transforms the accumulated spin precession into a measurable change in the fraction of spins in $|\uparrow\rangle$ that is read out via a projective measurement. (B) The produced entanglement is illustrated by the growth of the Rényi entropy S2 (19), which reaches a maximum after the first ODF drive. The second application of the ODF realizes a many-body echo of



the initial dynamics and disentangles the spin and the oscillator—demonstrated by the vanishing Rényi entropy after the second ODF drive—while also acting to map the small spin-independent displacement β into a spin rotation of $\phi=2g\tau\beta/\sqrt{N}$ about \hat{z} . (**C**) A phase-space illustration of the sequence. The initial state (leftmost panels) features the characteristic Gaussian and isotropic quantum noise distribution of a coherent state in both the spin and the oscillator degrees of freedom. The center panels illustrate that the entanglement can be interpreted as squeezing of the composite spin-oscillator quantum noise in a coupled basis. A phase-space illustration of the final decoupled state $|\psi_f\rangle$ is shown at the right. In (B) and (C) we use typical values of $g\tau=2$ for illustration.

echo: The displacement of the COM mode is encoded into a collective spin rotation of angle $\phi=2g\tau\beta/\sqrt{N},$ which can be read out by simple collective spin measurements (23, 32–34). Accounting for quantum projection noise of the collective spin, which limits angular resolution of small rotations to $\Delta\phi\!\geq\!1/\sqrt{N},$ the displacement can thus be estimated with a sensitivity $(\Delta\beta)^2=1/(4g^2\tau^2)$ that approaches the Cramer-Rao bound for $g\tau\gg 1.$ Moreover, we note that the form of the collective spin rotation is independent of the initial state of the phonons and hence is insensitive to any thermal occupation of the COM mode.

Displacement sensing

Assessing the performance of the implemented displacement-sensing protocol (Fig. 3), we see that the achievable sensitivity of the current experiment is primarily, but not fundamentally, limited by small shot-to-shot fluctuations of the COM mode frequency away from resonance as a consequence of impurity ions in the crystal and thermal occupation of the in-plane modes (35). These fluctuations limit our ability

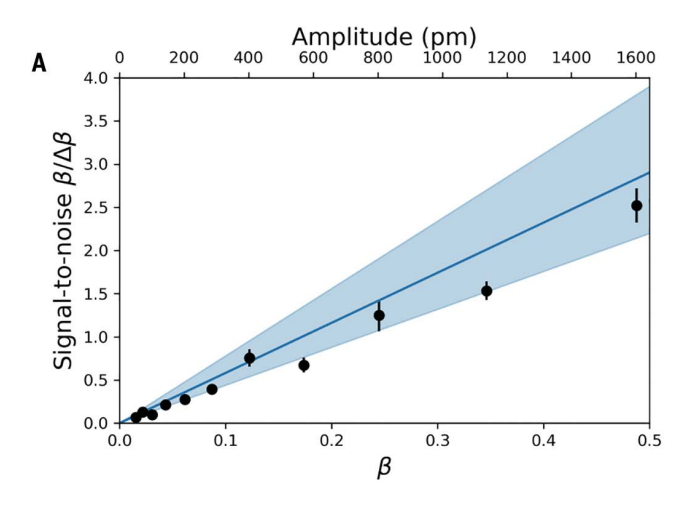
to perfectly reverse the entangling dynamics. Including COM frequency fluctuations with a root-mean-square spread $\sigma,$ as well as single-particle decoherence of the spins at rate Γ due to light scattering generated by the applied ODF beams and an initial thermal occupation $\bar{n}\approx 5$ of the COM mode, the signal-tonoise ratio (SNR) of a single measurement of β is reduced to

$$\begin{split} \frac{\frac{\beta}{\Delta\beta} = }{\sqrt{1 + \exp(-2\Gamma\tau)\left[(2\bar{n} + 1)g^2\sigma^2\tau^4 + \frac{4}{9}g^4\sigma^2\tau^6\right]}} \end{split} \tag{4}$$

(19). Physically, the prefactor $\exp(-\Gamma\tau)$ comes from depolarization of the collective spin due to decoherence, whereas the τ^4 and τ^6 terms of the denominator describe residual spin-phonon entanglement and excess projection noise introduced by the imperfect time reversal. In Fig. 3A, we find good agreement between the experimentally determined SNR and the theoretical prediction (Eq. 4) with independently calibrated values of g, σ , and Γ (19), justifying

our understanding of the various noise processes. In particular, we observe $\beta/\Delta\beta\to 0$ as $\beta\to 0$, which indicates that there are no additional systematic errors from effects beyond the applied displacement.

To assess the performance of the displacementsensing protocol, we determine the variance $(\Delta\beta)^2$ of a single measurement as a function of the ODF interaction time τ for a small fixed displacement β = 0.24. Again, we find good agreement with the theoretical estimates of $(\Delta\beta)^2$ presented in Fig. 3B. Optimizing over τ , we demonstrate a sensitivity of $(\Delta \beta)^2 = 3.3 \times$ 10^{-2} , or 8.8 ± 0.4 dB below the SQL. We emphasize that no technical noise has been subtracted in obtaining this result. Our result can be recast in terms of the absolute physical displacement Z_c of the COM mode using the relation $Z_{\rm c}=2z_0\beta/\sqrt{N}$, where $z_0=\sqrt{\hbar/(2m\omega_z)}$ is the size of the ground-state motional wave function of a single ion and the enhancement proportional to \sqrt{N} arises from the increased mass of the COM mode when more ions are present. Accounting for the 8-ms duration (e.g., accounting for preparation and readout) of a single measurement, we equivalently determine



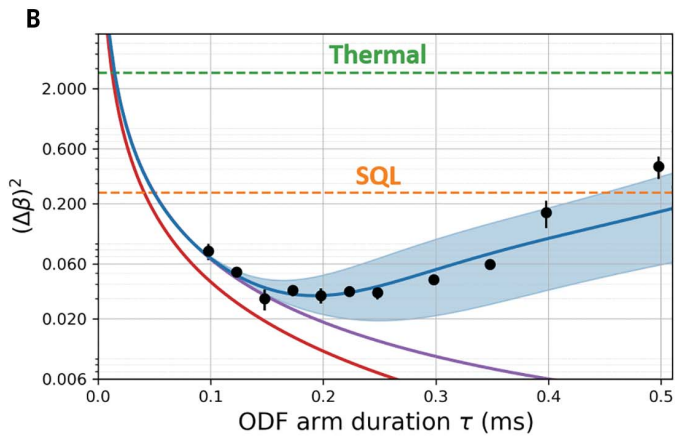


Fig. 3. Performance of mechanical displacement sensor. (**A**) Signal-to-noise ratio $\beta/(\Delta\beta) \equiv Z_c/(\Delta Z_c)$ as a function of displacement β (amplitude $Z_c \equiv 2z_0\beta/\sqrt{N}$, where $z_0 = \sqrt{\hbar/(2m\omega_z)}$ is the spatial extent of the ground-state wave function). Each experimental data point (black markers; error bars indicate statistical and systematic uncertainty) corresponds to the SNR of a single measurement with fixed $\tau = 200~\mu s$. Good agreement is found with the theoretical model (blue line) using independently calibrated values of $g/(2\pi) = 3.91~kHz$ and COM frequency fluctuations of $\sigma/(2\pi) = 40~Hz$. The shaded area indicates the confidence region for $\sigma/(2\pi) \in [20, 60]~Hz$, as well as spin depolarization characterized by $\Gamma = 500~s^{-1}$. The theoretical calculation also includes an observed 18% increase in background noise above the expected projection noise (19). (**B**) Sensitivity ($\Delta\beta$)² to the dimensionless displacement β as a function of ODF duration τ . Experimental data

(black markers; error bars indicate statistical and systematic uncertainty) is obtained from a small fixed physical displacement $Z_c = 775 \pm 28$ pm with a single-measurement SNR of ~1. We compare the observations to the theoretical predictions of an idealized model (red line), a model that includes depolarization due to spin decoherence (purple line, $\Gamma = 610 \text{ s}^{-1}$), and a model that also includes COM fluctuations of $\sigma = 40$ Hz (solid blue line); the shaded area indicates the confidence region for $\sigma/(2\pi) \in [20, 60]$ Hz. The SQL $(\Delta\beta)_{SQL}^2 = \frac{1}{4}$, corresponding the extent of the ground-state wave function, is indicated by a dashed orange line. For completeness, we also indicate the classically attainable sensitivity when accounting for excess thermal fluctuations, $\bar{n} = 5$ at the Doppler cooling limit $(\Delta\beta)_{th}^2 = (2\bar{n} + 1)(\Delta\beta)_{SQL}^2$ (dashed green line). The optimal experimental sensitivity of 8.8 ± 0.4 dB below the SQL (~19 dB below the thermal noise limit) corresponds to the average of the five points centered around $\tau = 200$ us (19).

that the optimal sensitivity is $\Delta Z_c = 36 \pm 1.5 \ \mathrm{pm/\sqrt{Hz}}$. Note that in the absence of our time-reversal protocol, excess projection noise introduced by the thermal occupation of the phonon mode, $\bar{n} \approx 5$, would have limited the achievable sensitivity to $(\Delta \beta)_{\mathrm{th}}^2 = (2\bar{n}+1)(\Delta \beta)_{\mathrm{SQL}}^2$ (19), or ~19 dB worse than our result.

Electric field sensing

Our ability to resonantly drive a small displacement of the COM mode over a long period of time, while maintaining a stable phase lock to a resonant ODF drive that generates spin-phonon entanglement, places our experiment in an excellent position for quantum-enhanced measurements of weak AC electric fields at the frequency of the COM mode.

In the protocol for sensing an electric field (Fig. 4), a fixed AC voltage is applied to an endcap electrode to drive a continuous displacement of the COM mode for a total time T. Simultaneously, an ODF drive is initially turned on for a time $\tau \leq T/2$ to generate spin-boson entanglement. At some later time, a second ODF pulse with inverted coupling $g \to -g$ (realized again by a π pulse about \hat{x} of the spins after the first ODF drive) is applied for an identical duration τ and timed to finish with the conclusion of the COM displacement. Collectively, the dynamics of the system is described by the modified Hamiltonian

$$\hat{H}_{\mathrm{sens}} = \hat{H}_{\mathrm{ODF}}(t) + i\eta \Big(\hat{a} - \hat{a}^{\dagger}\Big)$$
 (5)

(19), where η is a parameter related to the electric field to be measured. Note that the time dependence of $\hat{H}_{\text{ODF}}(t)$ indicates the modulation $g \to g(t)$.

For comparison purposes and to emphasize the quantum advantage, we compare the above protocol with a purely "classical" scheme where the continuous displacement of the COM mode is similarly applied for a total time T but we use only a single ODF drive for readout. Such a protocol ideally gives the sensitivity $(\Delta\eta)_C^2 = (1+g^2\tau^2)/[g^2\tau^2(2T-\tau)^2]$, which is always worse than the SQL defined as $(\Delta\eta)_{\rm SQL}^2 = 1/(4T^2)$. Note that the total displacement of the oscillator is ideally $\beta \equiv \eta T$. In contrast, our quantum-enhanced sensing scheme leads to $(\Delta\eta)^2 = 1/\left[4g^2\tau^2(T-\tau)^2\right]$, which yields sub-SQL scaling $(\Delta\eta)^2 \to 4/(g^2T^4)$ for $g\tau = gT/2 \gg 1$.

Figure 4 shows the experimentally obtained single-measurement electric field sensitivity of our protocol, in comparison to the SQL and the classical scheme. The ODF duration τ is chosen by numerically optimizing the theoretically predicted sensitivity including technical noise due to COM fluctuations σ and the thermal phonon occupation \bar{n} (19). Under current experimental conditions, for intermediate driving time $T=538~\mu s$, the quantum protocol allows us to attain a sensitivity of ~4.0 ± 0.5 dB below the SQL. Moreover, we find that in contrast to the quantum protocol, which is ideally insensitive to the initial phonon state, the classical

scheme is strongly limited by thermal noise. Quantitatively, the quantum protocol provides a ~14 dB improvement in sensitivity relative to the comparable classical scheme, demonstrating that entanglement can provide not only a fundamental but also a practical advantage when all relevant noise sources are taken into account.

For long drive times ($T \gtrsim 1$ ms), we find that the sensitivity is ultimately bounded by COM frequency noise, $(\Delta \eta)^2 \ge \sigma^2 (2\bar{n} + 1)/4$ (19). Experimentally we determine a single-measurement sensitivity of $\Delta \varepsilon = 2.3 \pm 0.1 \,\mu\text{V m}^{-1}$ at $T = 1.14 \,\text{ms}$, in good agreement with theory (Fig. 4). Accounting for the total duration of the experimental trial, $T_{\rm shot}$ = 8.73 ms, we thus obtain a best electric field sensitivity of $\Delta E =$ $\Delta \varepsilon \sqrt{T_{\rm shot}} = 220 \pm 10 \text{ nV m}^{-1} / \sqrt{\text{Hz}}$. Averaging the three experimental results with the longest drive time T gives a sensitivity of $\Delta E = 240 \pm 10 \text{ nV m}^{-1} / \sqrt{\text{Hz}} \text{ at } \sim 1.6 \text{ MHz}. \text{ This}$ compares favorably with electric field sensors using Rydberg atoms (36) that can reach sensitivities of 5.5 $\mu V m^{-1}/\sqrt{Hz}$ (25) at frequencies on the order of 10 GHz, and also approaches the sensitivity of meter-length classical antennas (37) but in a micrometerscale device.

Conclusions and outlook

We have demonstrated a quantum-enhanced sensor of mechanical displacements and weak electric fields in a crystal composed of ~150

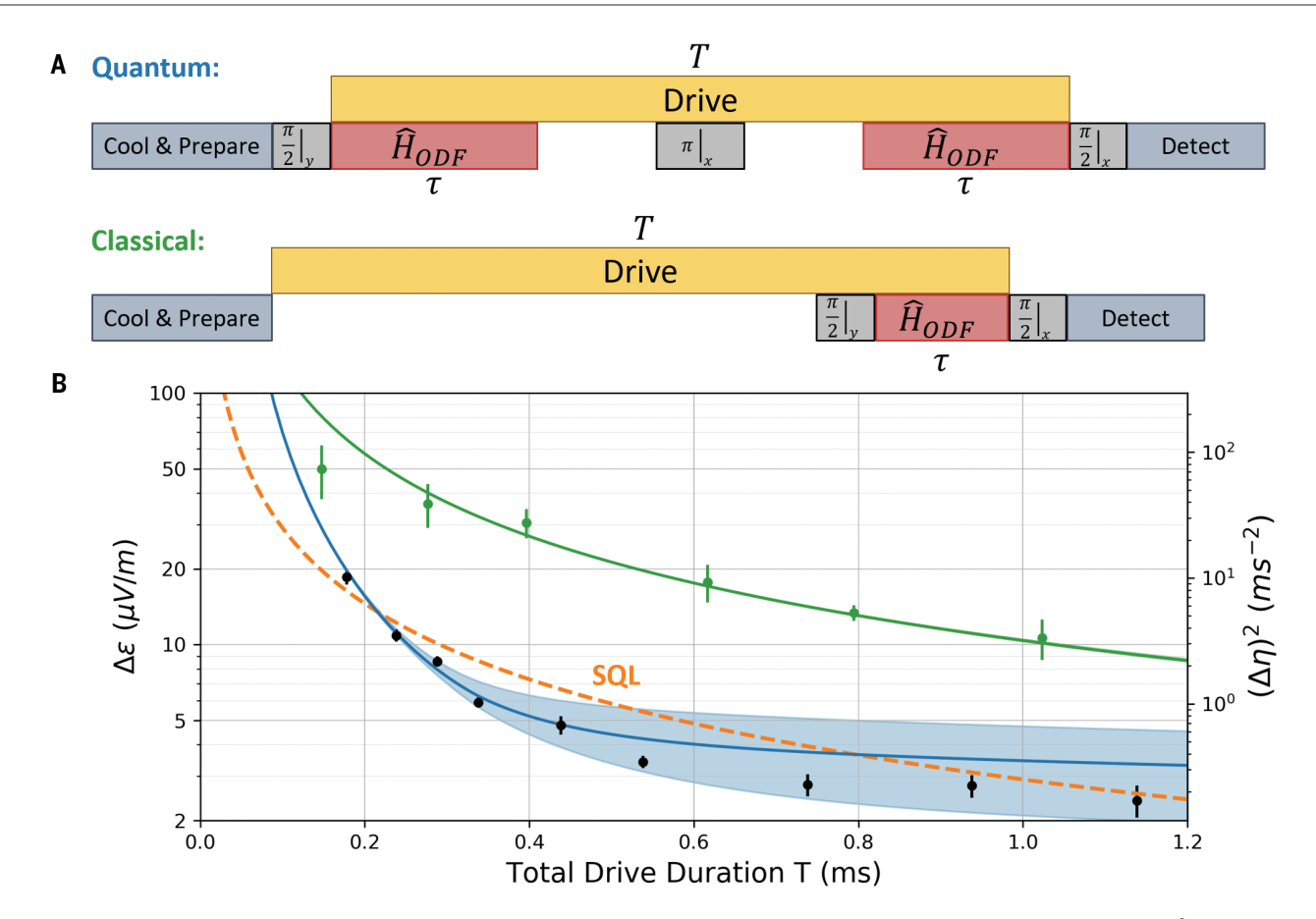


Fig. 4. Performance of the electric field sensor. (**A**) Schematic timeline of the quantum and classical protocols used to sense weak electric fields. The quantum protocol involves sequentially applying a pair of ODF drives with equal duration τ to first entangle and then disentangle the spin and motional degrees of freedom for readout via the spins, while a weak spin-independent drive is applied concurrently for a duration $T \ge 2\tau$. The classical protocol identically applies a spin-independent drive for duration T, but instead the ODF is only turned on for $\tau \le T$ at the end of the sequence to enable spin readout of the overall displacement. (**B**) Electric field sensitivity $\Delta \varepsilon$ [and $(\Delta \eta)^2$, right y axis] as a function of the total spin-independent drive duration T. We plot experimental data from both classical and quantum protocols (green and black markers, respectively; error bars indicate statistical and

systematic uncertainty) with τ chosen to ideally optimize $(\Delta\eta)^2$ (19). Good agreement is found with theoretical models of both protocols (green and blue solid lines) using independently calibrated values of $g/(2\pi)=3.88$ kHz and COM mode frequency fluctuations of $\sigma/(2\pi)\approx 40$ Hz, as well as $\Gamma=520$ s⁻¹. The shaded area indicates the confidence region of $\sigma/(2\pi)\in [20,60]$ Hz, which is not visible on this scale for the classical protocol. As reference, we contrast with the SQL $(\Delta\eta)_{SQL}^2=(2T)^{-2}$ (orange dashed line). Experimental data indicate that the quantum protocol attains a sensitivity that is optimally 4 dB below the SQL (19), or up to 14 dB better than the sensitivity attainable with the classical protocol. Taking the average of the three points with longest drive duration T results in an electric field sensitivity of $\Delta E=240\pm 10$ nV m⁻¹/ $\sqrt{\text{Hz}}$.

trapped ions. Currently, the primary limitations to the sensor's performance are COM frequency fluctuations and a thermal phonon population. However, these issues are not fundamental in nature and could be resolved in next-generation experiments. Indeed, feasible improvements to the stability of the COM mode frequency to the level of $\sigma/(2\pi)\approx 1$ Hz combined with a reduction of the phonon temperature via electromagnetically induced transparency (EIT) cooling, which has already been demonstrated in the same platform (38), should allow us to reach an electric field sensitivity of ~10 nV m⁻¹/ $\sqrt{\text{Hz}}$.

This degree of sensitivity could enable trappedion crystals as detectors of hidden photons and axions with a frequency (effective mass) compatible with the currently accessible range of COM mode frequencies (10 kHz to 10 MHz). Although comparisons to other state-of-theart platforms for sensing dark matter should be made carefully and consistently, one prominent advantage of the trapped-ion system is that the strong magnetic field required to couple axions to photons (18) is intrinsically present in the experimental platform. A further benefit is the capability to tune the COM frequency over the aforementioned range, which should be contrasted with dark matter searches using superconducting qubits in cavities (39) that must be operated near zero magnetic field and can be cumbersome to tune.

Our largest limitation is a finite-volume effect (40) that suppresses the axion-generated electric field because the characteristic size of the region over which the magnetic field is present is small relative to the long Compton wavelength of axions at typical COM frequen-

cies. The sensitivity of our experiment, which detects an electric field, is suppressed quadratically in this small ratio, whereas experiments that detect a dark matter-generated magnetic field are only suppressed to linear order (19). Nonetheless, even with this extra suppression. we estimate that our current platform with an electric field sensitivity of 10 nV m⁻¹/ $\sqrt{\text{Hz}}$ at 1.6 MHz could attain a sensitivity to axions with an axion-photon coupling as small as $g_{\alpha\gamma\gamma} \sim 1.6 \times 10^{-11}~{\rm GeV}^{-1}$ after 1 day of averaging (19). This is competitive with current experiments that search for axions at similar frequency scales, which have reported limits of $g_{\alpha\gamma\gamma} \lesssim 1 \times 10^{-11} \; \text{GeV}^{-1} \; (41, \, 42).$ Additional optimization of the trapped-ion platform, such as raising the ion number to $N \ge 10^6$ by the use of 3D crystals (43, 44) or increasing the size and strength of the superconducting magnetic

field, could also allow us to further enhance our sensing capability by as much as three orders of magnitude.

REFERENCES AND NOTES

- 1. J. P. Dowling, G. J. Milburn, Philos. Trans. R. Soc. A 361, 1655-1674 (2003).
- C. L. Degen, F. Reinhard, P. Cappellaro, Rev. Mod. Phys. 89, 035002 (2017).
- M. Tse et al., Phys. Rev. Lett. 123, 231107 (2019).
- Virgo Collaboration, Phys. Rev. Lett. 123, 231108 (2019).
- ADMX Collaboration, Phys. Rev. Lett. 120, 151301 (2018).
- L. Zhong et al., Phys. Rev. D 97, 092001 (2018). M. Malnou et al., Phys. Rev. X 9, 021023 (2019).
- K. M. Backes et al., Nature 590, 238-242 (2021). 8
- K. C. McCormick et al., Nature 572, 86-90 (2019). 10. F. Wolf et al., Nat. Commun. 10, 2929 (2019).
- 11. S. Schreppler et al., Science 344, 1486-1489 (2014). 12. S. Kolkowitz et al., Science 335, 1603-1606 (2012).
- 13. R. D. Delaney, A. P. Reed, R. W. Andrews, K. W. Lehnert,
- Phys. Rev. Lett. 123, 183603 (2019).
- 14. K. A. Gilmore, J. G. Bohnet, B. C. Sawyer, J. W. Britton, J. J. Bollinger, Phys. Rev. Lett. 118, 263602 (2017).
- 15. W. Wang et al., Nat. Commun. 10, 4382 (2019).
- 16. M. Affolter, K. A. Gilmore, J. E. Jordan, J. J. Bollinger, Phys. Rev. A **102**, 052609 (2020).
- 17. R. A. Thomas et al., Nat. Phys. 17, 228-233 (2021).
- 18. M. S. Turner, Phys. Rep. 197, 67-97 (1990).
- 19. See supplementary materials.
- 20. C. Hempel et al., Nat. Photonics 7, 630-633 (2013).
- 21. F. Toscano, D. A. R. Dalvit, L. Davidovich, W. H. Zurek, Phys. Rev. A 73. 023803 (2006).

- 22. M. Penasa et al., Phys. Rev. A 94, 022313 (2016).
- 23. R. J. Lewis-Swan et al., Phys. Rev. Lett. 124, 193602 (2020)
- 24. N. S. Kampel et al., Phys. Rev. X 7, 021008 (2017).
- 25. M. Jing et al., Nat. Phys. 16, 911-915 (2020).
- 26. S. C. Burd et al., Science 364, 1163-1165 (2019).
- 27. J. J. Bollinger, J. W. Britton, B. C. Sawyer, in Non-Neutral Plasma Physics VIII, AIP Conf. Proc. 1521 (2013), pp. 200-209.
- 28. B. C. Sawyer, J. W. Britton, J. J. Bollinger, Phys. Rev. A 89, 033408 (2014).
- 29. J. G. Bohnet et al., Science 352, 1297-1301 (2016).
- 30. A. Safavi-Naini et al., Phys. Rev. Lett. 121, 040503 (2018).
- 31. S. L. Braunstein, C. M. Caves, Phys. Rev. Lett. 72, 3439-3443
- 32. O. Hosten, R. Krishnakumar, N. J. Engelsen, M. A. Kasevich, Science 352, 1552-1555 (2016).
- 33. E. Davis, G. Bentsen, M. Schleier-Smith, Phys. Rev. Lett. 116, 053601 (2016).
- 34. S. P. Nolan, S. S. Szigeti, S. A. Haine, Phys. Rev. Lett. 119, 193601 (2017).
- 35. A. Shankar et al., Phys. Rev. A 102, 053106 (2020).
- 36. A. Facon et al., Nature 535, 262-265 (2016).
- 37. D. H. Meyer, Z. A. Castillo, K. C. Cox, P. D. Kunz, J. Phys. At. Mol. Opt. Phys. 53, 034001 (2020).
- 38. E. Jordan et al., Phys. Rev. Lett. 122, 053603 (2019).
- 39. A. V. Dixit et al., Phys. Rev. Lett. 126, 141302 (2021).
- 40. S. Chaudhuri et al., Phys. Rev. D 92, 075012 (2015).
- 41. J. A. Devlin et al., Phys. Rev. Lett. 126, 041301 (2021).
- 42. C. P. Salemi et al., arXiv 2102.06722 [hep-ex] (12 February 2021).
- 43. W. M. Itano et al., Science 279, 686-689 (1998).

44. A. Mortensen, E. Nielsen, T. Matthey, M. Drewsen, Phys. Rev. Lett. 96, 103001 (2006).

ACKNOWLEDGMENTS

We thank J. Thompson and A. Shankar for helpful discussions, and J. Teufel and K. Cox for careful review of our manuscript. Funding: Supported by US Department of Energy (DOE), Office of Science, National Quantum Information Science Research Centers, Quantum Systems Accelerator (QSA), a DOE Office of Science HEP QuantISED award, AFOSR grants FA9550-18-1-0319 and FA9550-20-1-0019, by DARPA and ARO grant W911NF-16-1-0576, the DARPA ONISQ program, ARO single investigator award W911NF-19-1-0210, NSF grants PHY1820885, JILA-PFC PHY-1734006, and QLCI-2016244, and NIST. Author contributions: K.A.G., M.A., E.J., and J.J.B. collected and analyzed the experimental data, R.J.L.-S., D.B., and A.M.R. developed the theoretical model. All authors discussed the results and contributed to the preparation of the manuscript. Competing interests: The authors declare no competing interests. Data and materials availability: All data needed to evaluate the conclusions of this study are provided in the main text or the supplementary materials.

SUPPLEMENTARY MATERIALS

science.sciencemag.org/content/373/6555/673/suppl/DC1 Supplementary Text Figs. S1 to S11 References (45-55)

15 March 2021; accepted 25 June 2021 10.1126/science.abi5226



Quantum-enhanced sensing of displacements and electric fields with twodimensional trapped-ion crystals

Kevin A. GilmoreMatthew AffolterRobert J. Lewis-SwanDiego BarberenaElena JordanAna Maria ReyJohn J. Bollinger

Science, 373 (6555), • DOI: 10.1126/science.abi5226

Quantum enhanced sensing

Harnessing quantum mechanical effects is expected to provide an advantage over classical sensing technology. By entangling the center-of-mass motional state of approximately 150 ions trapped in a two-dimensional Coulomb crystal with their collective spin state, Gilmore *et al.* demonstrate a quantum-enhanced measurement sensitivity of displacement and electric field. Such enhanced sensitivity could, for instance, find application in probing proposed weak interactions between dark matter and normal matter, as well as enhancing gravitational wave detection. —ISO

View the article online

https://www.science.org/doi/10.1126/science.abi5226 **Permissions**

https://www.science.org/help/reprints-and-permissions

Use of think article is subject to the Terms of service